Supporting Information

Xing et al. 10.1073/pnas.1314690111

SI Materials and Methods

Surgery and Preparation. Acute experiments were performed on adult Old World monkeys (*Macaca fascicularis*). All surgical and experimental procedures were performed in accordance with the guidelines of the US Department of Agriculture and were approved by the University Animal Welfare Committee at the New York University. Animals were sedated with midazolam (0.3 mg/kg, i.m.) and anesthetized initially with ketamine (30 mg/kg, i.m.) and then with isoflurane [1.5–3.5% (vol/vol) in air] after intubation. After i.v. catheters were placed in both hind limbs, the animal was placed in a stereotaxic frame and maintained on opioid anesthetic (sufentanil citrate, 6–12 $\mu g \cdot kg^{-1} \cdot h^{-1}$, i.v.) during further surgery. A craniotomy (~5 × 7 mm) was made in one hemisphere posterior to the lunate sulcus (~15 mm anterior to the occipital ridge, ~10 mm lateral from the midline) for recording from the primary visual cortex (V1). A small opening in the dura (~3 × 5 mm) was made to provide access for multiple electrodes. After surgery, anesthesia was maintained with a continuous infusion of sufentanil citrate (6–12 $\mu g \cdot kg^{-1} \cdot h^{-1}$, i.v.), and the animal was paralyzed with vecuronium bromide (0.1 $mg \cdot kg^{-1} \cdot h^{-1}$, i.v.). Hydration was maintained by infusing fluid at a rate of ~6 $mL \cdot kg^{-1} \cdot h^{-1}$. [The infusion rate was adjusted hourly to keep the urine specific gravity within the normal range (~1.010 g/mL).] Vital signs, including heart rate, electroencephalogram, blood pressure, and oxygen level in blood were closely monitored throughout the experiment. Expired carbon dioxide partial pressure was maintained close to 32–38 mmHg, and rectal temperature was kept at a constant 37 °C with the use of a feedback-controlled heating pad. A broad-spectrum antibiotic (Bicillin; 50,000 international units per kilogram, i.m.) and anti-inflammatory steroid (dexamethasone, 0.5 mg/kg, i.m.) were given on the first day and every 24 h during the experiment. The eyes were treated with 1% atropine sulfate solution to dilate the pupils and with a topical antibiotic (gentamicin sulfate, 3%) before being covered with gas-permeable contact lenses. Foveae were mapped onto a tangent screen using a reversing ophthalmoscope. The visual receptive fields of isolated neurons were later mapped on the same tangent screen, keeping reference to the foveae. Proper refraction was achieved by placing corrective lenses in front of the eyes on custom-designed lens holders. The eyes were stabilized with ophthalmic rings to minimize drift of visual field position.

Electrophysiological Recordings and Data Acquisition. A matrix of seven independently moveable electrodes (Thomas Recording) was used to record cortical population activity [multiunit activity (MUA) and local field potential (LFP)] simultaneously from multiple sites in V1. The seven electrodes were arranged in a straight line with each electrode separated from its neighbor by ~300 μm. Each electrode consisted of a platinum/tungsten core (25 μm in diameter and 1 μm at the tip) covered with an outer quartz-glass shank (80 μm in diameter) and had an impedance value of 1–4 MΩ. The multielectrode matrix was precisely positioned before recordings so the tip of the matrix was ~3 mm above the cortical surface. To keep all seven electrodes at roughly similar cortical depth, we independently moved each electrode from the surface of V1 until we obtained from each electrode a detectable high frequency response (multiunit hash) that was driven by the visual stimulus. Usually, this step provided a very good estimation of the upper part of layer 2/3 and helped us to align all seven electrodes at a similar cortical depth (Fig. 5*A* for example). Once all electrodes were placed in the superficial layer of V1, we built a chamber with bone wax to surround the multielectrode matrix and filled the chamber with agar to seal the craniotomy entirely. We found this procedure enhanced the stability of recordings throughout the experiment. Then, we conducted our experiments by advancing the electrode matrix at ~100-μm intervals in the cortex. This procedure allowed simultaneous recordings of multiple sites within the same cortical layer, all at nearby visual eccentricities. Electrical signals from the seven electrodes were amplified, digitized, and filtered (0.3–10 kHz) with a preamplifier (Tucker-Davis Technologies; model no. RA16SD) configured for multichannel recording. The Tucker-Davis system was interfaced to a computer (Dell) running a multichannel version of the OPEQ program (designed by J. A. Henrie, New York University, New York) to acquire both spike and LFP data. Visual stimuli were generated also with the custom OPEQ program running in a Linux computer (Dell) with a graphics card with Open GL optimization. Data collection was synchronized with the screen refresh to a precision of <0.01 ms. Stimuli were displayed on a 20-inch CRT monitor (IIyama HM 204DTA flat color graphic display; pixels: 1024 × 768; frame rate: 100 Hz; mean luminance: 59.1 cd/m^2) with a screen-viewing distance of ~114 cm. Thus, the display screen subtended 20° × 15° visual angle. The basic attributes of single cells at each site were estimated using small drifting sinusoidal gratings surrounded by a gray background (both the gratings and the gray background had a mean luminance of 59.1 cd/m^2).

Signal Processing for LFP and Multiunit Activity. The LFP is defined as the low-pass-filtered (300 Hz) continuous signal recorded by each microelectrode and MUA is defined as follows: high-pass-filtered (1,000 Hz) raw signal was half-wave-rectified in the negative direction; then, the mean and SD for the half-wave-rectified signal were estimated; MUA was finally defined as the number of events 3 SDs more negative than the mean.

Visual Stimuli. The stimulus consisted of a sequence of alternating black and white squares (1) (8° × 8°) against a gray background (luminance: 59.1 cd/m^2). The luminance of white and black squares was adjusted so the contrasts of the light increment (luminance: 107.3 cd/m^2) and light decrement (luminance: 11.1 cd/m^2) with the background were nearly equal. Each black or white square appeared for 500 ms, and the entire sequence lasted ~4 or ~8 s.

Cycle-Averaged Responses. MUA or the LFP was aligned by the onset of the black or white stimulus for each cycle. For each recording site, MUA and the LFP to black or white stimuli at each time delay were calculated and averaged across stimulus cycles (Fig. 1 *B* and *C*, *Right*). To minimize the effect of adaptation, we excluded the first stimulus cycle in the analysis. We defined the cycle-averaged responses, $R_{black}(t)$ and $R_{white}(t)$, as the mean MUA or LFP across different cycles. The spontaneous response for each recording site, $R_{spontaneous}$, is defined as the site's average responses to a gray background (luminance: 59.1 cd/m^2) before stimulus onset.

Signal/Noise Ratio. We used the signal/noise ratio of the cycle-averaged MUA and LFP to determine whether or not a recording site had a stimulus-driven signal that was out of the noise. Signal/noise ratio for MUA was defined as the peak difference of the visual evoked MUA and spontaneous MUA divided by the SD of the spontaneous MUA. Signal/noise ratio for LFP was defined as the peak difference of the visual evoked LFP and spontaneous LFP divided by the SD of the spontaneous LFP. The signal/noise

ratio was calculated for the MUA and LFP from each recording site as in the following equations:

$$\mathrm{MUA\_SN_{white}} = \left(\max\left(\mathrm{MUA_{white}}\right) - \mathrm{mean}\left(\mathrm{MUA_{spontaneous}}\right)\right) / \mathrm{std}\left(\mathrm{MUA_{spontaneous}}\right) \ldots, \quad \textbf{[S1]}$$

$$\mathrm{MUA\_SN_{black}} = \left(\max\left(\mathrm{MUA_{black}}\right) - \mathrm{mean}\left(\mathrm{MUA_{spontaneous}}\right)\right) / \mathrm{std}\left(\mathrm{MUA_{spontaneous}}\right) \ldots, \quad \textbf{[S2]}$$

$$\mathrm{LFP\_SN_{white}} = \mathrm{abs}\left(\min\left(\mathrm{LFP_{white}}\right) - \mathrm{mean}\left(\mathrm{LFP_{spontaneous}}\right)\right) / \mathrm{std}\left(\mathrm{LFP_{spontaneous}}\right) \ldots, \quad \textbf{[S3]}$$

$$\mathrm{LFP\_SN_{black}} = \mathrm{abs}\left(\min\left(\mathrm{LFP_{black}}\right) - \mathrm{mean}\left(\mathrm{LFP_{spontaneous}}\right)\right) / \mathrm{std}\left(\mathrm{LFP_{spontaneous}}\right) \ldots. \quad \textbf{[S4]}$$

We included a recording site in the population averages if any of the four signal/noise ratios were larger than 2.

Histology. Cells were assigned to different layers of V1 based on the results of track reconstruction (2–4). Along each track, we recorded the depths of every recording site during the experiment and then made three to four electrolytic lesions at 600- to 900-μm intervals at the end of the experiment. A lesion was made by passing a 3-μA direct current for 2 s through the quartz-insulated platinum/tungsten microelectrodes (Thomas Recording) with a stimulus generator (ALA Scientific Instruments; model no. STG-1001). After euthanasia, the animal was perfused through the heart with 1 L of heparinized saline (0.01 M PBS) followed by 2–3 L of fixative (4% paraformaldehyde, 0.25% glutaraldehyde in 0.1 M phosphate buffer). After the brain was blocked and sectioned at 50 μm, the lesions were initially located in unstained sections and then the lesion sections were stained for cytochrome oxidase. Cytochrome oxidase provides good anatomical localization of the laminar boundaries. Cortical layers were determined based on the cell density and cytochrome oxidase-specific labeling (5). After locating the lesions within the sections, we reconstructed the electrode penetration using a camera lucida and determined the location of each recorded site relative to the reference lesions and the layers of the cortex. Our estimate of cortical depths of recording sites was quite precise: the difference between the estimated unit distance between lesion sites and the physical unit distance between two parallel electrodes was less than 5% of the average unit distance from the two measures. Therefore, factors such as the shrinkage of the brain section did not affect our estimates substantially. The mean thickness of each layer was then used to determine each cell's normalized cortical depth ranging from 0 (representing the surface) to 1 (representing the boundary between layer 6 and the white matter).

1. Moore BD, 4th, Kiley CW, Sun C, Usrey WM (2011) Rapid plasticity of visual responses in the adult lateral geniculate nucleus. *Neuron* 71(5):812–819.
2. Hawken MJ, Parker AJ, Lund JS (1988) Laminar organization and contrast sensitivity of direction-selective cells in the striate cortex of the Old World monkey. *J Neurosci* 8(10): 3541–3548.
3. Xing D, Yeh CI, Shapley RM (2009) Spatial spread of the local field potential and its laminar variation in visual cortex. *J Neurosci* 29(37):11540–11549.
4. Yeh CI, Xing D, Williams PE, Shapley RM (2009) Stimulus ensemble and cortical layer determine V1 spatial receptive fields. *Proc Natl Acad Sci USA* 106(34): 14652–14657.
5. Wong-Riley M (1979) Columnar cortico-cortical interconnections within the visual system of the squirrel and macaque monkeys. *Brain Res* 162(2):201–217.

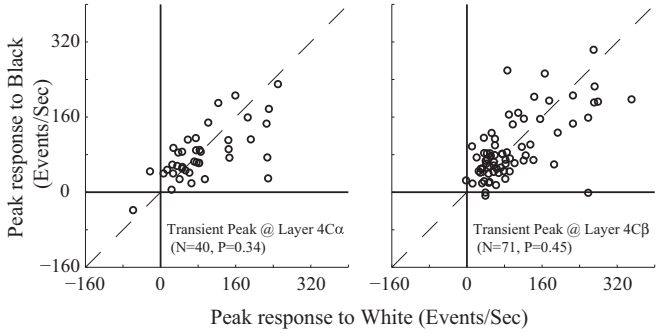

Fig. S1. Peak transient MUA to black and white stimuli (individual recording sites). Peak amplitude of transient MUA to white (*x* axis) and to black (*y* axis) stimuli were compared in layer 4Cα ($n = 40$) (*Left*) and layer 4Cβ ($n = 71$) (*Right*).

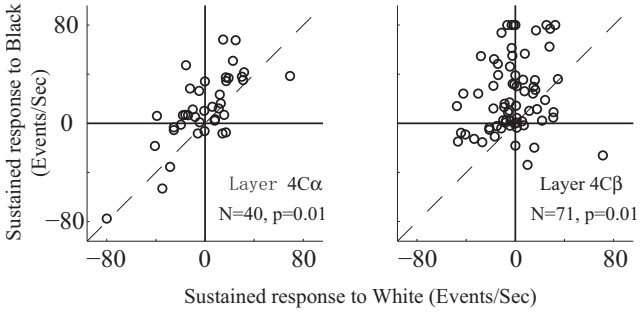

Fig. S2. Average sustained MUA to black and white stimuli (individual recording sites). Mean sustained MUA to white (*x* axis) and to black (*y* axis) stimuli were compared in layer 4Cα ($n = 40$) (*Left*) and layer 4Cβ ($n = 71$) (*Right*).